Magnetoresonant Raman scattering in zinc-blende-type semiconductors: Electron-phonon interaction mediated by a deformation potential

V. López* and G. E. Marques
Departamento de Física, Universidade Federal de São Carlos, 13566-905, São Carlos, SP, Brazil

J. Drake and C. Trallero-Giner
Departamento de Física Teórica, Universidad de La Habana, 10400 C. Habana, Cuba

(Received 2 September 1997)

The one-phonon Raman scattering efficiency for III-V and II-VI zinc-blende-type semiconductors in high magnetic fields including the valence-band admixture has been obtained. The coupling of the heavy-hole and light-hole valence bands has been taken into account through the Luttinger-Kohn Hamiltonian model. The Raman profiles are calculated as a function of magnetic field B_0 and laser frequency ω_L with a deformation-potential type of electron-phonon interaction. The influence on the Raman tensor of the nonparabolicity as well as the anisotropic behavior of Landau ladders in terms of magnetic field and the z component of the hole wave vector are analyzed. Explicit expressions for the Raman scattering efficiency as a function of ω_L, B_0, and the Luttinger-Kohn parameters are given. The dependence of the lifetime broadening on the laser incident energy, magnetic field, and Landau quantum number of the intermediate electronic states has been considered in the Raman scattering efficiency. Based on these grounds, the essential features of recent magneto-Raman experiments in bulk GaAs, using the crossed polarization geometries $\overline{z}(\sigma^{\pm},\sigma^{\mp})z$ can be explained. [S0163-1829(97)04547-5]

I. INTRODUCTION

Raman spectroscopy has become one of the most powerful techniques used in the analysis of aspects of the electronic structure, the vibrational normal modes and their interaction with the quasiparticles in semiconductor crystals. Resonant Raman scattering occurs whenever the energy of an incident or scattered photon equals the energy of an intermediate electronic state. Application of external magnetic field produces an enhancement in the Raman sensitivity due to the one-dimensional character of the density of states as introduced by the field.[1] The study of the intensity of the Stokes LO-phonon Raman scattering as a function of the magnetic field strength gives detailed information about the band structure of the crystal. Strong resonances may appear near the singular points of the electronic density of states.

The use of different scattering configurations in a Raman process provides information about the symmetry of the electron-phonon interaction and different contributions to the scattering may appear from deformation-potential or Fröhlich forms of interactions based on the selection rules that govern these processes. In the crossed polarization geometries, $\overline{z}(\sigma^{\pm},\sigma^{\mp})z$, the transitions are assisted by deformation-potential interactions while in parallel geometries, $\overline{z}(\sigma^{\pm},\sigma^{\pm})z$, the electron-phonon coupling occurs via the Fröhlich Hamiltonian. In this work we will be concerned with just the former scattering geometries. Interesting results can be obtained once the energy of the incident and scattered light simultaneously approaches the energy of electronic transitions for a given value of the magnetic field strength. In this case the intermediate electronic transitions, which are in general virtual, become real and the Raman scattering efficiency is strongly enhanced. This is the so-called doubly resonant Raman scattering.

Normally, simple parabolic models have been used in the theoretical studies of one-phonon magneto-Raman scattering.[1] Due to the degeneracy of the light- and heavy-hole bands near the Γ point in the Brillouin zone, this model is only a rough approximation. More realistic models to calculate the electronic structure of a crystal are needed in order to take into account the mixing of valence levels and the coupling between valence and conduction levels. This is important in the study of transport and optical properties of semiconductors and in Raman spectroscopy particularly, since the effects of the valence-band admixture are strong for a wide range of energy of the incident light.

Another approach has been used frequently concerning the phenomenological lifetime broadening of the intermediate electron-hole pair states, which is usually taken as a constant. In the framework of this paper we calculate the enhancement of the broadening due to the electron-phonon Fröhlich interaction, which yields a new picture of the resonance spectra due to its dependence on the electron (hole) wave vector and on the corresponding Landau level indexes. Some resonant features in the calculated spectra may either disappear or become too weak, thus leading to more realistic pictures of the magnetoresonant scattering efficiency.

II. BASIC HAMILTONIAN AND WAVE FUNCTION

We consider the system in a homogeneous magnetic field **B** parallel to the z axis and the Landau gauge where $\mathbf{A}=(0,xB_0,0)$, for the vector potential, is chosen. The electronic states in semiconductors with zinc-blende symmetry and under applied magnetic field can be written as a sum of the product of Bloch states and harmonic oscillator wave functions, which may contain a considerable degree of mixture.[2,3] One of the realistic models mentioned before that

treats the electronic structure of heavy- and light-hole states in a magnetic field and takes into account their strong mixture is the Luttinger-Kohn Hamiltonian model,[4,5] which provides a good description for the valence-band states in those semiconductors where the spin-orbit, Δ_0, and the band-gap energies, E_g, are large (say E_g, $\Delta_0 \geqslant 300$ meV). For such a situation, the full $\mathbf{k}\cdot\mathbf{p}$ Kane-Weiller Hamiltonian model[6] can be separated into two 2×2 matrices with Γ_7^{SO} [split-off (SO) band] and Γ_6^c (conduction band) symmetries, or the so-called parabolic models, and into a 4×4 matrix with Γ_8^v (top valence band) symmetry.[4]

The Γ_6^c and Γ_7^{SO} bands will be characterized by effective masses (m_c, m_{SO}) and Landé g factors (g_c, g_{SO}) in the simple parabolic model where the interactions with the light-hole (lh) and heavy-hole (hh) bands are neglected. In this manner the coupling between hh and lh ladders, due to the Γ_8^v degeneracy at the Γ point is included through the 4×4 Luttinger Hamiltonian. Schematically the full Hamiltonian can be written as

$$\hat{H}=\begin{bmatrix} H_{cc} & 0 & 0 \\ 0 & H_{vv} & 0 \\ 0 & 0 & H_{ss} \end{bmatrix}, \tag{1}$$

where each parabolic block has the form

$$H_{cc}=E_g+\frac{\hbar^2\hat{k}^2}{2m_c}+\frac{1}{2}g_c\mu_B\boldsymbol{\sigma}\cdot\mathbf{B}, \tag{2}$$

$$H_{ss}=-\Delta_0-\frac{\hbar^2\hat{k}^2}{2m_{\mathrm{SO}}}+\frac{1}{2}g_{\mathrm{SO}}\mu_B\boldsymbol{\sigma}\cdot\mathbf{B}, \tag{3}$$

and where the Luttinger-Kohn Hamiltonian can be written as a compact form

$$\begin{aligned} H_{vv}=-\frac{\hbar^2}{2m_0}\Big\{ & \gamma_1\hat{k}^2+\gamma_2\left[\left(\frac{1}{3}J^2-J_x^2\right)\hat{k}_x^2+\text{c.p.}\right] \\ & -4\gamma_3[\{J_xJ_y\}\{\hat{k}_x\hat{k}_y\}+\text{c.p.}] \\ & +2\kappa\mu_BJ_zB_0+2q_{\mathrm{LK}}J_z^3B_0\Big\}, \end{aligned} \tag{4}$$

where c.p. stands for cyclic permutations of (x,y,z).

In these expressions, μ_B is the Bohr magneton, $\boldsymbol{\sigma}$ is the Pauli matrix, $\gamma_1,\gamma_2,\gamma_3,\kappa,q_{\mathrm{LK}}$ are the Luttinger parameters, m_0 is the bare electron mass, and J_i $(i=x,\ y,\ z)$ are matrices for the components of the angular momentum, respectively. In Eqs. (2)–(4) the magnetic interaction is included in the wave-vector operator $\mathbf{k}=[-i\nabla+(e/c\hbar)\mathbf{A}]=(\hat{k}_x,\hat{k}_y,\hat{k}_z)$.

The eigenfunctions and eigenvalues for the $\{\Gamma_6^c,\Gamma_7^{\mathrm{SO}}\}$ manifolds described by Eqs. (2) and (3) could be found elsewhere.[5] For the Γ_8^v band, analytical bulk solutions of the Schrödinger equation corresponding to the Hamiltonian (4) can be obtained if no warping effect $(\gamma_2\simeq\gamma_3)$ is considered and the axial approximation $(q_{\mathrm{LK}}\simeq0)$ is taken into account.

In this case the 4×4 Hamiltonian H_{vv} is block diagonalized into two independent 2×2 blocks for the heavy- and light-hole states. They can be written as

$$H_{vv}=\begin{bmatrix} (\gamma_1\pm\gamma_2)\hbar\omega_c\left(\hat{N}+\frac{1}{2}\right)+(\gamma_1\mp2\gamma_2)\dfrac{\hbar^2\hat{k}_z^2}{2m_0}+\hbar\omega_c\left(\frac{1}{2}\pm1\right)\kappa & -\sqrt{3}\,\overline{\gamma}\hbar\omega_c\hat{a}^2 \\ -\sqrt{3}\,\overline{\gamma}\hbar\omega_c\hat{a}^{\dagger2} & (\gamma_1\mp\gamma_2)\hbar\omega_c\left(\hat{N}+\frac{1}{2}\right)+(\gamma_1\pm2\gamma_2)\dfrac{\hbar^2\hat{k}_z^2}{2m_0}-\hbar\omega_c\left(1\mp\frac{1}{2}\right)\kappa \end{bmatrix}, \tag{5}$$

where $\hat{N}=\hat{a}^+\hat{a}$ is the number operator, $\hat{a}$ $(\hat{a}^\dagger)$ is the annihilation (creation) operator defined as $\hat{a}=\sqrt{\hbar c/2eB_0}(\hat{k}_x+i\hat{k}_y)$, $\overline{\gamma}=[(\gamma_2+\gamma_3)/2]$, $\omega_c=(eB_0/cm_0)$ is the cyclotron frequency. The eigenvalues of these two matrices in Eq. (5), E_{N,k_z}^i, are given by

$$\begin{aligned} E_{N,k_z}^{1,2}=&\ \alpha_-(N)+\gamma_1\left(\frac{\hbar^2k_z^2}{2m_0}\right) \\ & \pm\sqrt{\left[\beta_-(N)-2\overline{\gamma}\left(\frac{\hbar^2k_z^2}{2m_0}\right)\right]^2+c(N)}, \end{aligned} \tag{6}$$

$$\begin{aligned} E_{N,k_z}^{3,4}=&\ \alpha_+(N)+\gamma_1\left(\frac{\hbar^2k_z^2}{2m_0}\right) \\ & \pm\sqrt{\left[\beta_+(N)-2\overline{\gamma}\left(\frac{\hbar^2k_z^2}{2m_0}\right)\right]^2+c(N)}, \end{aligned} \tag{7}$$

with $N=0,1,2,\ldots$ for the eigenstates E_{N,k_z}^1, E_{N,k_z}^4 and $N=2,3,\ldots$ for eigenstates E_{N,k_z}^2, E_{N,k_z}^3, respectively. The other coefficients in the above expressions are defined as

$$\alpha_\mp(N)=\hbar\omega_c\left[\gamma_1\left(N-\frac{1}{2}\right)\mp\left(\overline{\gamma}-\frac{1}{2}\kappa\right)\right], \tag{8}$$

$$\beta_\mp(N)=\hbar\omega_c\left[\overline{\gamma}\left(N-\frac{1}{2}\right)\mp(\gamma_1-\kappa)\right], \tag{9}$$

$$c(N)=3\,\overline{\gamma^2}N(N-1)\hbar\omega_c. \tag{10}$$

The full calculated spectrum consists of four Landau ladders where E_{N,k_z}^2, E_{N,k_z}^4 are heavy-mass states and E_{N,k_z}^1, E_{N,k_z}^3 are light-mass states. Due to the admixture of the valence band, these Landau ladders will not be equidistant anymore and one cannot classify them according to their heavy or light hole character at the Γ_8^v point, as is normally done in parabolic models. However, the labels heavy- or light-hole only correspond to their behavior for $B_0\to0$ or $k_z\to\infty$. In

general, the effective mass of each layer is a function of the component k_z, the magnetic field strength B_0, and the Landau level number N.

Let us define the dimensionless parameter $x=\sqrt{\hbar k_z^2/(2m_0\omega_c)}$, which is a measure of the ratio between the kinetic energy for the motion along the magnetic field and the cyclotronic energy of the motion in the plane perpendicular to the magnetic field. The general form of the eigenstates in Eq. (5) is a linear combination of functions $|N;J,J_z\rangle$, which are formed by the product of the one-dimensional harmonic oscillator function $|N\rangle$ and the periodic Bloch function with symmetry Γ_8^v, represented as $|J,J_z\rangle$. Here, J is the total angular momentum and J_z its z component, which takes the values $J=\frac{3}{2}$ and $J_z=-\frac{3}{2},-\frac{1}{2}$, for the spin-down components and $J_z=+\frac{1}{2},+\frac{3}{2}$, for the spin-up components. These linear combinations can be written as

$$|\Psi_1\rangle=a_{11}(N,k_z)\left|N-2;\frac{3}{2},\frac{3}{2}\right\rangle+a_{21}(N,k_z)\times\left|N;\frac{3}{2},-\frac{1}{2}\right\rangle\overset{x\to\infty}{\to}|N;lh^-\rangle, \tag{11}$$

$$|\Psi_2\rangle=a_{12}(N,k_z)\left|N-2;\frac{3}{2},\frac{3}{2}\right\rangle+a_{22}(N,k_z)\times\left|N;\frac{3}{2},-\frac{1}{2}\right\rangle\overset{x\to\infty}{\to}|N-2;hh^+\rangle, \tag{12}$$

$$|\Psi_3\rangle=a_{13}(N,k_z)\left|N-2;\frac{3}{2},\frac{1}{2}\right\rangle+a_{23}(N,k_z)\times\left|N;\frac{3}{2},-\frac{3}{2}\right\rangle\overset{x\to\infty}{\to}|N-2;lh^+\rangle, \tag{13}$$

$$|\Psi_4\rangle=a_{14}(N,k_z)\left|N-2;\frac{3}{2},\frac{1}{2}\right\rangle+a_{24}(N,k_z)\times\left|N;\frac{3}{2},-\frac{3}{2}\right\rangle\overset{x\to\infty}{\to}|N;hh^-\rangle, \tag{14}$$

where each weight $a_{ij}(N,k_z)$ that measures the mixtures of pure states is given by

$$a_{11}=-a_{22}=\left[\frac{1}{2}+\frac{1}{2}\frac{\beta_-(N)-\overline{\gamma\hbar}^2k_z^2/m_0}{\sqrt{[\beta_-(N)-\overline{\gamma\hbar}^2k_z^2/m_0]^2+c(N)}}\right]^{1/2}, \tag{15}$$

$$a_{12}=a_{21}=\left[\frac{1}{2}-\frac{1}{2}\frac{\beta_-(N)-\overline{\gamma\hbar}^2k_z^2/m_0}{\sqrt{[\beta_-(N)-\overline{\gamma\hbar}^2k_z^2/m_0]^2+c(N)}}\right]^{1/2}, \tag{16}$$

$$a_{13}=-a_{24}=\left[\frac{1}{2}-\frac{1}{2}\frac{\beta_+(N)-\overline{\gamma\hbar}^2k_z^2/m_0}{\sqrt{[\beta_+(N)-\overline{\gamma\hbar}^2k_z^2/m_0]^2+c(N)}}\right]^{1/2}, \tag{17}$$

TABLE I. Parameters for GaAs used in this work, from Refs. 1 and 13.

Parameters	GaAs
γ_1	6.85
γ_2	2.1
γ_3	2.9
E_G (meV)	1519
Δ_0 (meV)	341
κ	1.2
q_{LK}	0.04
g_c	−0.32
$g_{\rm SO}$	4.5
m_c (m_0)	0.0665
$m_{\rm SO}$ (m_0)	0.170
$\hbar\omega_{\rm LO}$ (meV)	37

$$a_{14}=a_{23}=\left[\frac{1}{2}+\frac{1}{2}\frac{\beta_+(N)-\overline{\gamma\hbar}^2k_z^2/m_0}{\sqrt{[\beta_+(N)-\overline{\gamma\hbar}^2k_z^2/m_0]^2+c(N)}}\right]^{1/2}. \tag{18}$$

For those eigenstates with $N=0$ and $N=1$, the weights $a_{11}(N,k_z)$ and $a_{12}(N,k_z)$ in Eqs. (11) and (12) and $a_{13}(N,k_z)$ and $a_{14}(N,k_z)$ in Eqs. (13) and (14) are identically zero. Therefore, in these two Landau levels the eigenstates $|\Psi_1\rangle$, $|\Psi_2\rangle$, $|\Psi_3\rangle$, and $|\Psi_4\rangle$ will become just pure states with degenerated spin-down components. For $N\geqslant 2$ all four eigenstates will have a mixture of spin-up and spin-down pure states.

Let us now calculate the eigenvalues and the eigenstates and show the form of the mixture as a function of the parameter x, defined earlier, for different Landau ladders, inside the bulk of GaAs, whose general band parameters are given in Table I.

Figure 1 shows the calculated energy levels within the Luttinger-Kohn model, as a function of dimensionless parameter x and for selected values of the Landau quantum number N. The nonparabolic behavior for low quantum numbers in the range $x\leqslant 3$ can be clearly seen (that is high magnetic field and/or low values of the kinetic energy $\hbar^2k_z^2/2m_0$). Furthermore, the heavy-mass behavior of E^2_{N,k_z} and E^4_{N,k_z} ladders is characterized in the figure by the narrower spaced levels at $x\geqslant 3$. For the same range of x, the ladders E^1_{N,k_z} and E^3_{N,k_z} show the light-mass behavior as represented by the widely spaced energy levels. For the sake of comparison we have also included the first two pure state energies for light-mass (dotted lines) and heavy-mass (dash-dotted lines) particles, as obtained from a diagonal approximation (parabolic case) in dotted lines. At large values of x, they show clearly the different curvatures according to their masses.

A better quantitative idea about the effect of the mixing between the Γ_8^v valence bands can be observed in Fig. 2, where the weight factors $|a_{ij}|^2$ $(i=1,2)$ $(j=1,2,3,4)$ are shown as a function of x and for different values of the Landau number N. As already said before, for $N<2$, the

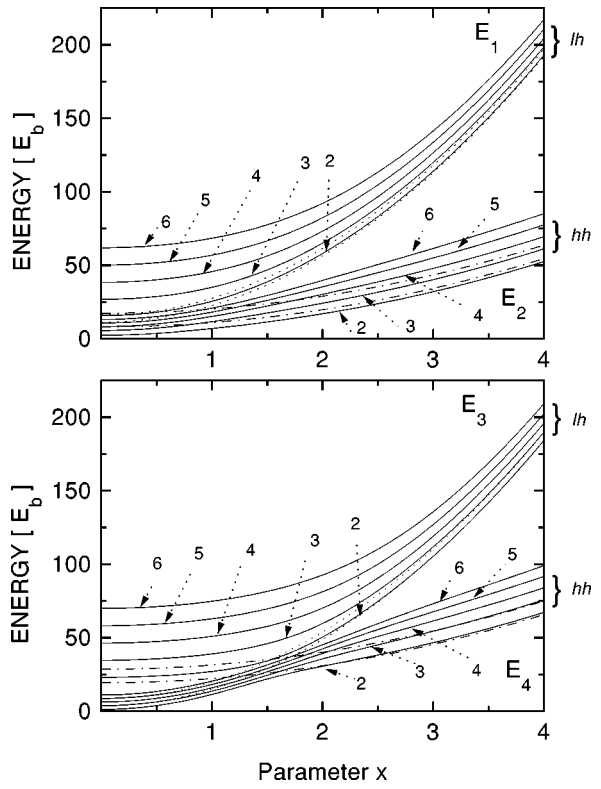

FIG. 1. Energy ladders E_j $(j=1-4)$ in magnetic units of $\hbar\omega_c$ $(E_b=E_i/\hbar\omega_c)$ are shown as a function of dimensionless parameter $x=\sqrt{\hbar k_z^2/(2m_0\omega_c)}$ for the Landau quantum numbers $N=2,3,4,5,6$. The calculation has been performed for GaAs semiconductors with input parameters given in Table I. The admixed ladders are represented by solid lines while the parabolic dispersion law (for $N=2,3$) is by shown dash-dotted lines for heavy-mass ladders and dotted line for light-mass ladders.

states are pure or parabolic but, for $N\geqslant 2$, pure heavy- or light-mass states are only obtained in the limit $x\to\infty$ where the mixing disappears completely. In this limit, the effective masses can be treated as constants, as was considered in Ref. 1, in the evaluation of the one-phonon resonant Raman scattering in III-V semiconductors. A slightly different approach has also been done in the limit of $k_z=0$ $(x=0)$ (Ref. 1) by considering a partial mixing between the Γ_8^v valence bands. In that model, which was justified by the divergency of the electronic density of states, the coefficients a_{ij} $(i=1,2)$ $(j=1,2,3,4)$ were independent on k_z while, in the energy ladders, the dependence on k_z was included as simply parabolic.

III. RAMAN SCATTERING EFFICIENCY

The Raman scattering efficiency $(dS/d\Omega)$ per unit length and unit solid angle is given by

$$\frac{dS}{d\Omega}=\left[\frac{\omega_L\omega_S^3\eta_L\eta_S^3}{(2\pi c^2)^2}\right]\left(\frac{V}{(\hbar\omega_L)^2}\right)|W_{FI}(\omega_S,\mathbf{e}_S;\omega_L,\mathbf{e}_L)|^2, \tag{19}$$

where $\eta_j,\omega_j,\mathbf{e}_j$ $(j=L,S)$ are the refractive index, frequency, and polarization vector of the laser (L) and scattered (S) light fields, respectively, c is the speed of light, and V is the volume of the crystal. In Eq. (19), W_{FI} is the scattering amplitude which, for the one-phonon process in the lowest order perturbation theory, can be written as[1]

$$W_{FI}=\sum_{\alpha,\beta}\frac{\langle F|\hat{H}_{E-R}|\alpha\rangle\langle\alpha|\hat{H}_{E-P}|\beta\rangle\langle\beta|\hat{H}_{E-R}|I\rangle}{(\hbar\omega_S-E_\alpha+i\Gamma_\alpha)(\hbar\omega_L-E_\beta+i\Gamma_\beta)}, \tag{20}$$

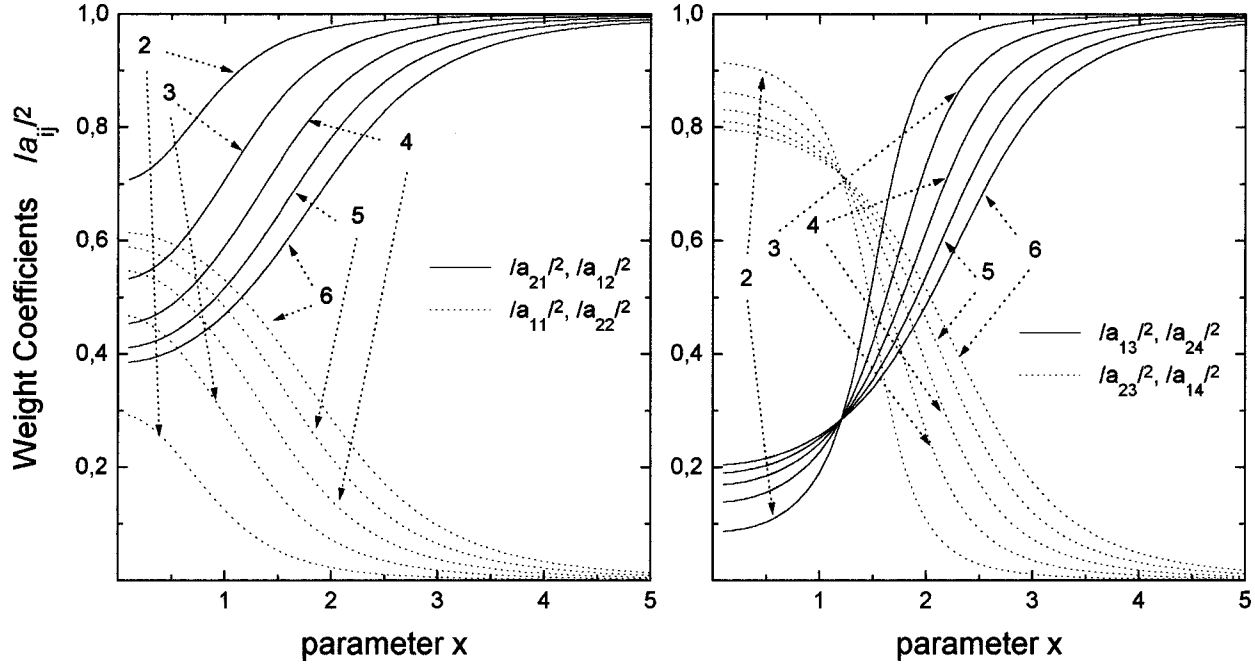

FIG. 2. Weight coefficients $|a_{ij}|^2$ of the admixed wave functions $|\Psi_j\rangle$ calculated as a function of $x=\sqrt{\hbar k_z^2/(2m_0\omega_c)}$, for different Landau quantum number $N=2,3,4,5,6$. The coefficients $|a_{11}|^2$, $|a_{22}|^2$,$|a_{23}|^2$,$|a_{14}|^2$ are indicated by dotted lines and $|a_{12}|^2$,$|a_{21}|^2$, $|a_{13}|^2$,$|a_{24}|^2$ by solid lines.

with $|I\rangle$ and $|F\rangle$ being the initial and final states corresponding to the scattering of an incident photon of frequency ω_L by a phonon of frequency $\omega_{\rm LO}$ and followed by the emission of a photon of frequency $\omega_S=\omega_L-\omega_{\rm LO}$. Also, α and β refer to intermediate electron-hole pair states with energies E_α, E_β and lifetime broadening Γ_α and Γ_β, respectively. Furthermore, $\hat{H}_{E\text{-}R}$ and $\hat{H}_{E\text{-}P}$ are the electron-radiation and electron-phonon interaction Hamiltonians defined in the framework of the second quantization by

$$\hat{H}_{E\text{-}R}=\sum_{\boldsymbol{\kappa},\mathbf{e},\mu,\mu'}\left(\frac{e}{m_0}\sqrt{\frac{2\pi\hbar}{\eta^2\omega V}}\right)\times[\mathbf{e}\langle\mu'|e^{i\boldsymbol{\kappa}\cdot\mathbf{r}}\mathbf{p}|\mu\rangle\ \hat{d}^\dagger_{\mu'}\hat{d}_\mu\hat{a}_{\boldsymbol{\kappa},\mathbf{e}}+\text{H.c.}], \tag{21}$$

and

$$\hat{H}_{E\text{-}P}=\sum_{\mathbf{q},\mu,\mu'}[S^{\mu'}_{\mu}\ \hat{d}^\dagger_{\mu'}\hat{d}_\mu\ \hat{b}_{\mathbf{q}}+\text{H.c.}]. \tag{22}$$

In these expressions, $\hat{a}_{\boldsymbol{\kappa},\mathbf{e}}$ ($\hat{a}^\dagger_{-\boldsymbol{\kappa},\mathbf{e}}$), $\hat{d}_\mu$ ($\hat{d}^+_{\mu'}$) and $\hat{b}_{\mathbf{q}}$ ($\hat{b}^\dagger_{-\mathbf{q}}$) are the annihilation (creation) operators for photons, electron-hole pairs, and phonons, respectively, $\boldsymbol{\kappa}$ ($\mathbf{q}$) represents the photon (phonon) wave vector, $\mathbf{p}$ is the momentum operator, and $S^{\mu'}_{\mu}$ is the coupling constant between an electron-hole pair and a phonon. For the case of deformation-potential interaction, $S^{\mu'}_{\mu}$ can be written as[7]

$$S^{\mu'}_{\mu}(\mathbf{q})=\left(\frac{u_0\sqrt{3}}{2a_0}\right)[\langle\mu'|\mathbf{D}_e(\mathbf{r}_e)e^{-i\mathbf{q}\cdot\mathbf{r}_e}-\mathbf{D}_h(\mathbf{r}_h)e^{-i\mathbf{q}\cdot\mathbf{r}_h}|\mu\rangle], \tag{23}$$

with a_0 being the lattice constant, $u_0=\sqrt{\hbar V_c/(2V\omega_{\rm LO}M^*)}$ is the zero-point amplitude of the relative sublattice displacement, V_c is the volume of the primitive cell, M^* is the reduced mass of the atoms contributing to the optical modes, and $\mathbf{D}_\alpha(\mathbf{r}_\alpha)$ ($\alpha=e$ for electrons and h for holes) is the deformation potential constant as defined by Bir and Pikus.[8]

In our band model consisting of one conduction band, the deformation-potential interaction cannot couple the electron band due to the s character of the Γ^c_6 symmetry, which gives $\langle\Gamma^c_6|\mathbf{D}_e|\Gamma^c_6\rangle=\mathbf{0}$.

In the Faraday configuration and for circularly polarized light with $\mathbf{e}=(\mathbf{e}_x\pm i\mathbf{e}_y)/\sqrt{2}$ for the $\sigma^\pm$ polarization, respectively, the one-phonon Raman scattering, mediated by the deformation-potential interaction, is possible in the scattering configurations $\overline{z(\sigma^\pm,\sigma^\mp)z}$, where the [001] direction has been chosen as the quantization axis parallel to $\boldsymbol{\kappa}$.[1] The deformation-potential mechanism yields nonzero contributions for those states that couple split-off or light-hole levels to heavy-hole ones. Therefore, the selection rules between pure states, represented as $|\frac{3}{2},\pm\frac{3}{2}\rangle$ for heavy-hole, $|\frac{3}{2},\pm\frac{1}{2}\rangle$ for light-hole, and $|\frac{1}{2},\pm\frac{1}{2}\rangle$ for split-off states, are given by

$$\overline{z(\sigma^+,\sigma^-)z}\quad\overline{z(\sigma^-,\sigma^+)z}$$

$$|\tfrac{3}{2},\tfrac{3}{2}\rangle\rightarrow|\tfrac{3}{2},-\tfrac{1}{2}\rangle\ \ |\tfrac{3}{2},-\tfrac{3}{2}\rangle\rightarrow|\tfrac{3}{2},\tfrac{1}{2}\rangle$$

$$|\tfrac{3}{2},\tfrac{1}{2}\rightarrow|\tfrac{3}{2},-\tfrac{3}{2}\rangle\ \ |\tfrac{3}{2},-\tfrac{1}{2}\rangle\rightarrow|\tfrac{3}{2},\tfrac{3}{2}\rangle \tag{24}$$

$$|\tfrac{1}{2},\tfrac{1}{2}\rangle\rightarrow|\tfrac{3}{2},-\tfrac{3}{2}\rangle\ \ |\tfrac{1}{2},-\tfrac{1}{2}\rangle\rightarrow|\tfrac{3}{2},\tfrac{3}{2}\rangle$$

$$\tfrac{3}{2},\tfrac{3}{2}\rangle\rightarrow|\tfrac{1}{2},-\tfrac{1}{2}\rangle\ \ |\tfrac{3}{2},-\tfrac{3}{2}\rangle\rightarrow|\tfrac{1}{2},\tfrac{1}{2}\rangle.$$

For dipole-allowed interband optical transitions we obtain, for the Landau quantum number $\Delta N=0$, for the z component of the angular momentum changes by one ($\Delta J_z=\pm1$) in the $\sigma^\pm$ polarizations and the spin components remain unchanged ($\Delta m_s=0$).

By introducing expressions (21)–(23) into Eq. (20) and using the wave functions (11)–(14) together with the above selection rules, the scattering amplitude for the $\overline{z(\sigma^-,\sigma^+)z}$ configuration can be written as

$$W_{FI}=i|P|^2d_0A\sum_{N=0}^{\infty}\int_0^\infty dk_z\Bigg\{\frac{1}{\hbar\omega_S-E^+_{\rm SO^-}(k_z,k_z,N,N)+i\Gamma_{\rm SO^-}}\frac{2}{3}\sum_{i=1}^{2}\frac{|a_{1i}(N+2)|^2}{\hbar\omega_L-E^+_i(k_z,k_z,N,N+2)+i\Gamma_i}$$

$$+\frac{2}{3}\sum_{i=3}^{4}\frac{|a_{2i}(N)|^2}{\hbar\omega_S-E^-_i(k_z,k_z,N,N)+i\Gamma_i}\frac{1}{\hbar\omega_L-E^-_{\rm SO^+}(k_z,k_z,N,N)+i\Gamma_{\rm SO^+}}+\frac{1}{3}\sum_{i,j=1}^{2}\frac{|a_{2i}(N)|^2}{\hbar\omega_S-E^+_i(k_z,k_z,N,N)+i\Gamma_i}$$

$$\times\frac{|a_{1j}(N+2)|^2}{\hbar\omega_S-E^+_j(k_z,k_z,N,N+2)+i\Gamma_j}+\frac{1}{3}\sum_{i,j=3}^{4}\frac{|a_{2i}(N)|^2}{\hbar\omega_S-E^-_i(k_z,k_z,N,N)+i\Gamma_i}\frac{|a_{1j}(N+2)|^2}{\hbar\omega_L-E^-_j(k_z,k_z,N,N+2)+i\Gamma_j}\Bigg\}. \tag{25}$$

In the above expression, we have defined

$$A=\sqrt{\frac{3}{2}}\left(\frac{1}{m_0}\right)^2\left[\frac{e^3B_0}{\sqrt{\eta_L\eta_S}}\frac{1}{\sqrt{\omega_L\omega_S}}\right]\left(\frac{u_0}{\pi a_0 c}\right), \tag{26}$$

$$E_i^{\pm}(k_{z_e},k_{z_h},N_e,N_h)=[E_c^{\pm}(k_{z_e},N_e)-E_i(k_{z_h},N_h)],$$

$$i=1,2,3,4, \tag{27}$$

$$E_{\mathrm{SO}^{\pm}}^{\pm}(k_{z_e},k_{z_h},N_e,N_h)=[E_c^{\pm}(k_{z_e},N_e)-E_{\mathrm{SO}^{\pm}}(k_{z_h},N_h)], \tag{28}$$

$$E_c^{\pm}(k_{z_e},N_e)=E_g+\frac{\hbar^2k_{z_e}^2}{2m_c}+\hbar\omega_c^c\left(N_e+\frac{1}{2}\right)\pm\frac{1}{2}\mu_B g_c B_0, \tag{29}$$

$$E_{\mathrm{SO}^{\pm}}(k_{z_h},N_h)=\left[-\Delta_0+\frac{\hbar^2k_{z_h}^2}{2m_{\mathrm{SO}}}+\hbar\omega_c^{\mathrm{SO}}\left(N_h+\frac{1}{2}\right)\pm\frac{1}{2}\mu_B g_{\mathrm{SO}}B_0\right], \tag{30}$$

where, $\omega_c^{\mathrm{SO}}=(eB_0/cm_{\mathrm{SO}})$, $\omega_c^c=(eB_0/cm_c)$, and d_0 is the optical deformation-potential constant.

The expression for the $\overline{z}(\sigma^+,\sigma^-)z$ configuration can be obtained immediately by just replacing $\hbar\omega_L$ by $\hbar\omega_S$ and vice versa, and finally by changing the sign of W_{FI}.

New contributions from interband transitions are obtained in the framework of this model. The mixing leads to the appearance of new terms that cannot be achieved within a simple treatment of the electronic structure in a parabolic model. It is important to notice that, with strong band mixing, there are twelve different contributions that must be taken into account for each scattering configuration, instead of four within the parabolic model.

As was already pointed in Ref. 1, when the incident light is resonant with an interband magneto-optical electronic transition for a certain value of the magnetic field, the condition for incoming resonance is fulfilled. The outgoing resonance appears when the scattered light equals the energy difference for an interband transition from a conduction to a valence band. Due to the difference in the effective masses of each valence band, the condition for double resonance can be fulfilled, for certain values of the energy of the light. Before proceeding to the calculation of the Raman scattering, let us first calculate the broadening of intermediated states within the present model for the electronic structure.

IV. LIFETIME BROADENING CALCULATION

Even at very low temperature, different interactions may contribute to the lifetime broadening of the electronic intermediate states. In a magnetic field, even at temperature near 0 K, the effects of the electron-LO-phonon interaction may be very strong and the possibility of resonant coupling between different intraband states via one-phonon emission becomes real. This effect has strong influence on the magneto-Raman efficiency.

For electronic energy, $E=[\hbar^2k'_z2/2m+\hbar\omega_c(N_e+\frac{1}{2})]>\hbar\omega_{\mathrm{LO}}$, the emission of LO phonons by electrons (or holes) is not forbidden and the inverse of the electronic lifetime, γ, must be dominated by the electron-LO-phonon Fröhlich Hamiltonian. The relaxation time for LO phonons is of the order of 10^{-13} s. It is clear that the peaks observed in Raman scattering efficiency will be drastically reduced whenever the LO-phonon emission can be switched on. In Refs. 9 and 10 the electron (hole) lifetime broadening, determined by the LO-phonon interaction was calculated as a function of the electron (hole) wave vector and the Landau level index. The lifetime broadening is proportional to the probability per unit time, $W_{N\to N'}$ that the electron (hole) makes a transition from the state N'_e,k'_{z_e} (N'_h,k'_{z_h}) to the state N_e,k_{z_e} (N_h,k_{z_h}), accompanied by LO-phonon emission.

The total lifetime broadening $\gamma_{N_eN_h}$ for the electron-hole pair states, within the framework of the free-electron–hole approach, may be written as a simple sum of the electron and hole probabilities, that is,

$$\gamma_{N_eN_h}(k_e,k_h)=W^e_{N_e}(k_e)+W^h_{N_h}(k_h), \tag{31}$$

where

$$W^i_{N_i}(k_i)=\sum_{N'_i,k'_{z_i}}W_{N_i\to N'_i}(k'_{z_i})\,\delta\left[\left(\frac{\hbar^2k_{z_i}^2}{2m_i}\right)+\hbar\omega_{\mathrm{LO}}+\hbar\omega_c^i(N_i-N'_i)-\left(\frac{\hbar^2k_{z_i}'^2}{2m_i}\right)\right],\quad i=e,h. \tag{32}$$

Here, the following explicit expression for $W_{N_i\to N'_i}(k'_{z_i})$ has been obtained in Ref. 9:

$$W_{N_i\to N'_i}(k'_{z_i})=\alpha_i\omega_{\mathrm{LO}}\sqrt{\frac{\hbar\omega_{\mathrm{LO}}}{a_i}}\int_0^\infty e^{-t}F_{N'_i,N_i}(t)\{[t+(\sqrt{\hbar k_{x_i}^2/2m_i\omega_c^i}+\sqrt{a_i/\hbar\omega_c^i})^2]^{-1}[t+(\sqrt{\hbar k_{x_i}^2/2m_i\omega_c^i}-\sqrt{a_i/\hbar\omega_c^i})^2]^{-1}\}dt. \tag{33}$$

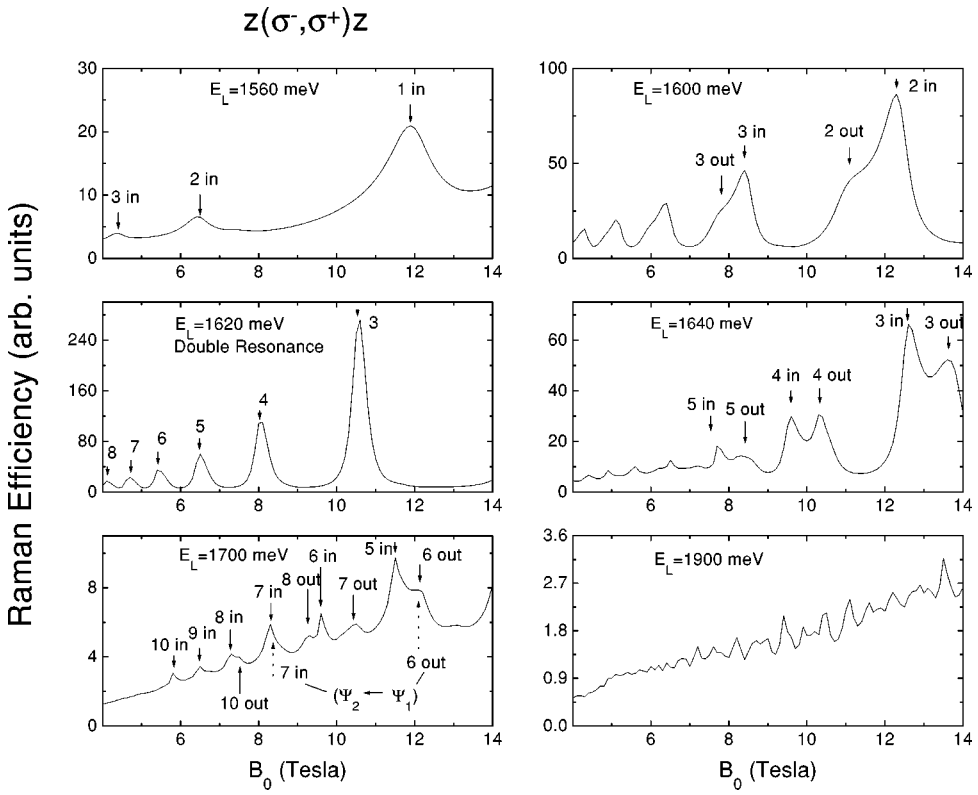

FIG. 3. The Raman intensity for bulk GaAs calculated as a function of the magnetic field for different energies of the incident light ($E_L=\hbar\omega_L$) in the $\overline{z}(\sigma^-,\sigma^+)z$ configuration. The arrows label the incoming or outgoing resonances for Landau quantum numbers N with stronger contributions (see text). The lifetime broadening was taken as a constant, with a value $\Gamma=1$ meV for all transitions.

In the above expression, we have defined

$$a_i=\left[\left(\frac{\hbar^2k_{z_i}^2}{2m_i}\right)+\hbar\omega_c^i(N_i-N_i')-\hbar\omega_{\rm LO}\right] \tag{34}$$

and

$$F_{N',N}(t)=\begin{cases}\dfrac{N'!}{N!}t^{N-N'}[L_{N'}^{N-N'}(t)]^2, & N\geqslant N'\\ \dfrac{N!}{N'!}t^{N'-N}[L_N^{N'-N}(t)]^2, & N'>N,\end{cases} \tag{35}$$

where $L_{N'}^{N-N'}$ are the Laguerre polynomials and α_e (α_h) the Fröhlich electron- (hole-) LO-phonon coupling constant.

The electron- (hole-) phonon coupling is switched off by conservation of energy if $[(\hbar^2k_{z_i}^2/2m_i)+\hbar\omega_c^i(N_i+\frac{1}{2})]\leqslant\hbar\omega_{\rm LO}$, $i=e,h,$SO, as can be seen from Eq. (32). Other processes that would also contribute to the lifetime, such as scattering by impurities and by acoustical phonons will be assumed as a constant broadening, γ_0, independent of k_z and N. That is, in the present model, the full broadening is

$$\Gamma_{NeNh}=(\gamma_0+\gamma_{NeNh.}). \tag{36}$$

These general results and their influence on the calculated magneto-Raman efficiency will be discussed in the next section.

V. RESULTS AND DISCUSSION

Let us now analyze the light scattering for the configuration $\overline{z}(\sigma^-,\sigma^+)z$ in GaAs, whose parameters are given in Table I.

The contribution of the first two terms in the sum inside the integral of W_{FI}, in Eq. (25), involves transitions between the split-off and the conduction-band states. Their relative contributions to the Raman tensor are important when the energy of the incident light, $\hbar\omega_L$, is near to $(E_g+\Delta_0)$, where the interband transitions become real. This can be seen in Fig. 3, where the magneto-Raman efficiency calculated at $\hbar\omega_L=1900$ meV is shown. For such an incident photon energy, the effect of the mixing is negligible for small values of the Landau level index N since the resonant transitions occur for large values of the hole kinetic energy ($x>3$), which corresponds to the parabolic limit involving pure eigenstates, as explained above.

For incident photons with energies in the range 1560−1700 meV (see Fig. 3), the effects produced by the mixing of the electronic states become strong for small values of the Landau level indexes, which requires low values of the hole kinetic energy at the resonance ($0\leqslant x\leqslant 2$). Here, as can be noticed in Fig. 2, the band mixing is in this considered range. Therefore, the strongest contribution to the Raman efficiency comes from the transition between the conduction band and the two valence band states allowed by the selection rules in Eq. (24), namely, $|\Psi_4\rangle\leftarrow|\Psi_3\rangle$, and that would only correspond to a hh^--like state ($|\Psi_4\rangle$) and an

lh^+-like state ($|\Psi_3\rangle$), respectively at values $x \to \infty$. One may see in Fig. 2 that several transitions occur due to the band mixing and some of them disappear for high hole kinetic energy or low magnetic field. In particular, the main contributions at energies below $\hbar\omega_L = 1700$ meV are associated to interband transitions between components $a_{14}|lh^+\rangle$ and $a_{23}|hh^-\rangle$ of involved states and is a direct consequence of the band mixing at $x \leqslant 2$.

What is commonly called the heavy or light character of a valence band states is determined by their behavior at low field or high kinetic energies, and they only correspond to the character associated to the effective mass in a certain range of energy. By following the selection rules in Eq. (24) we see that transitions between ''mixed states'' with character $c \leftarrow hh^- \leftarrow lh^+ \leftarrow c$ are forbidden in the $\overline{z}(\sigma^-,\sigma^+)z$ configuration. Within the parabolic model, the strongest contribution arises from the ''pure state'' transitions, $c \leftarrow hh^+ \leftarrow lh^- \leftarrow c$ for the same scattering configuration and range of energies. This transition also occur within the nonparabolic model but its contribution to the Raman efficiency is very small. The reason for such a difference between models is related to the fact that, in the nonparabolic model, the former allowed transitions between pure states become transitions between components of admixed states whose weight is not exactly one. For each allowed transition followed by selection rules between pure states the valence-band mixing allows new contributions between the Luttinger-Kohn states. It is important to notice that the character of these new transitions may not correspond to the character that they had in the parabolic case and it is caused by the band mixing enhanced by the magnetic field. The picture remains the same until the energy of the incident light is below 1700 meV. At $\hbar\omega_L > 1700$ meV, the states become almost pure and the effect of the mixing tends to disappear. This is a direct consequence of the wave-function dependence on the hole kinetic energy. For very high energies of the incident light the resonant transition occurs at high values of the hole kinetic energy for low Landau levels and the parabolic regime is completely recovered.

The condition for doubly resonant first-order Raman scattering is only completely fulfilled when the energy difference between two electronic transitions equals the energy $\hbar\omega_{LO}$ of the phonon involved in this process. Some suitable value of the magnetic field may produce the appropriate energy splitting necessary. For GaAs under applied magnetic filed, the resonances between incident and scattered lights coincide at $\hbar\omega_L \simeq 1620$ meV. At this energy, the electron-phonon deformation interaction couples the transitions between states $|\Psi_3\rangle \leftarrow |c\rangle$ (incoming resonance) and $|c\rangle \leftarrow |\Psi_4\rangle$ (outgoing resonance), leading to a maximum in the Raman intensity. There is still another chance for a double resonance, that is $|\Psi_2\rangle \leftarrow |\Psi_1\rangle$ transition near 1630 meV for the resonant coupling between the lh^- component of $|\Psi_1\rangle$ and the hh^+ component of $|\Psi_2\rangle$. Nevertheless, this contribution to the total intensity appears to be very small in the $\overline{z}(\sigma^-,\sigma^+)z$ configuration. The appearance of two different doubly resonant conditions is also an effect associated to the valence-band mixing, where the parabolic model predicts just one.

Another interesting effect of the band mixing is that heavy-hole components of the admixed states may have lower effective mass than the light-hole components. This effect is clearly seen in our results and the Fig. 1 shows the difference in the set of narrow (wide) spacing between levels for the heavy-mass (light-mass) carriers in the range $x < 3$, if compared to the parallel spacing between levels in the parabolic model with the heavy-mass particle above the light-mass one. This is present in the Luttinger-Kohn Hamiltonian, where heavy holes (light holes) with effective mass along the z direction defined by $m_z = 1/(\gamma_1 - 2\gamma_2)$ $[m_z = 1/(\gamma_1 + 2\gamma_2)]$ have the in-plane effective mass given by $m_{xy} = 1/(\gamma_1 + \gamma_2)$ $[m_{xy} = 1/(\gamma_1 - \gamma_2)]$ in appropriate units.

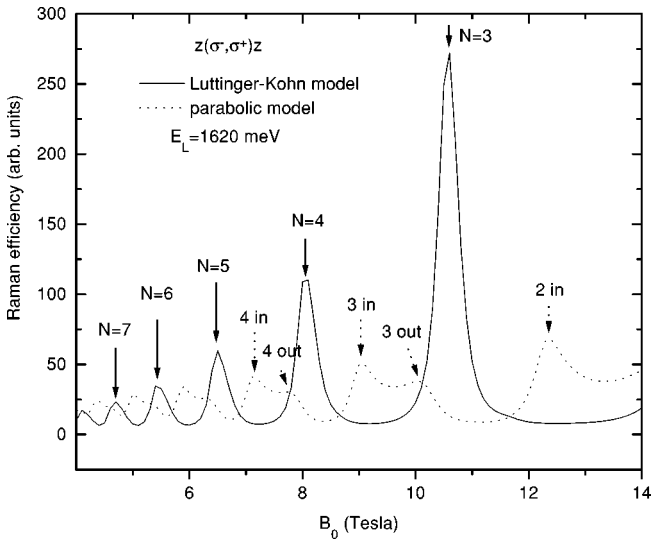

FIG. 4. Raman intensity vs magnetic field in bulk GaAs for an incident laser energy $E_L = 1620$ meV in the $\overline{z}(\sigma^-,\sigma^+)z$ configuration, calculated using admixed valence bands (solid line) and compared to the calculated spectrum using a parabolic model (dashed line). The broadening lifetime, $\Gamma = 1$ meV, was used for all electronic transitions.

The double resonance occurs just for a case where the hole effective mass at the incoming resonance is smaller than the effective mass of the outgoing one. Therefore, our model shows that the corresponding component $a_{23}|hh^-\rangle$ of $|\Psi_3\rangle$, at which the incoming transition occurs, indeed has an effective mass smaller than the mass of the component $a_{14}|lh^+\rangle$ of $|\Psi_4\rangle$ (involved in the outgoing transition). Simple parabolic models for the electronic structure could not explain such a resonance.

In order to further compare these models we show in Fig. 4 the calculated magneto-Raman profile in both models, where we have used a constant lifetime broadening for both cases. The strongest contribution in the parabolic model arises from the transition between the $hh^+ \leftarrow lh^-$ states. This contribution also appears for the admixed bands within the Luttinger-Kohn model but, in this case, the strongest resonances are due to transitions with character $hh^- \leftarrow lh^+$, which would be forbidden within a parabolic model in the $\overline{z}(\sigma^-,\sigma^+)z$ configuration. Furthermore, notice that the intensities of the resonant peaks are modulated by a quadratic decay dependence on the magnetic field strength [see Eqs. (19), (25), and (26)], and by the value of weight factors, $|a_{14}|^2$ and $|a_{23}|^2$, of each wave functions components calculated as a function of the magnetic field (see Fig. 2).

Some results, after applying the calculated lifetime broad-

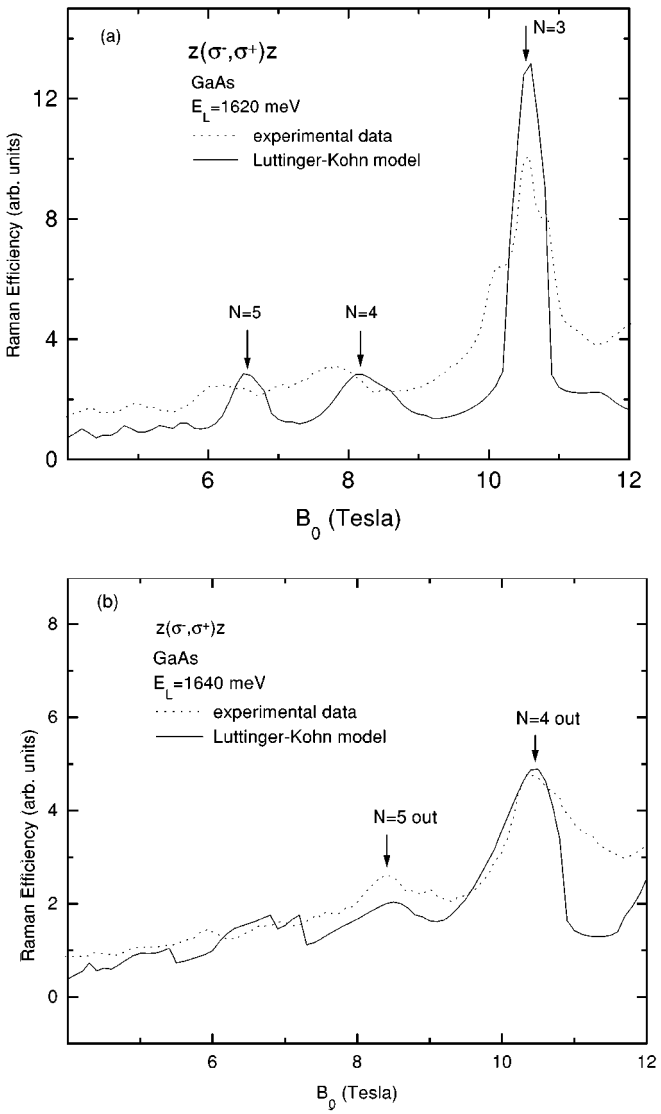

FIG. 5. Calculated magneto-Raman intensity (solid line) as a function of B_0, taking into account the lifetime broadening dependence on the Landau quantum number and the electron (hole) wave vector $\mathbf{k}_e$ ($\mathbf{k}_h$) [see Eqs. (31)–(35)]. The experimental result (dashed line) corresponds to the same value of the incident light energy and scattering configuration in GaAs crystals according to Ref. 11. In part (a) the incident photon has energy $E_L = 1620$ meV and, in part (b), $E_L = 1640$ meV.

ening for each intermediate state, as described in the last section to the Raman efficiency of Sec. IV are shown in parts (a) and (b) of Fig. 5 together with the experimental results of Ref. 11. One may see that the calculation of lifetime broadening and the electronic states within the Luttinger-Kohn model are two essential ingredients that provide an explanation for the relative heights and shape of each resonant peaks in the magneto-Raman efficiency. It is clear that the lifetime broadening dependence on the wave vectors and on Landau level indexes changes the picture of these resonances. If the results shown in Fig. 5 are compared with previous results of Fig. 4 for the same energy of the incident light one see that some of the shapes of resonant become wider and tend to disappear. In this way our model can better explain the relative heights and shape of the different resonance peaks ex-

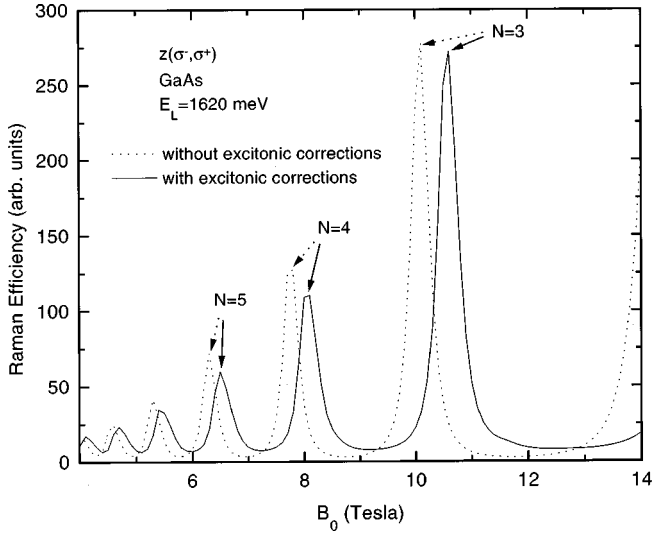

FIG. 6. Raman intensity vs magnetic field in bulk GaAs for an incident laser energy $E_L = 1620$ meV in the $\overline{z}(\sigma^-,\sigma^+)z$ configuration, calculated with (solid line) and without (dotted line) the excitonic corrections in the high-field limit. The broadening lifetime, $\Gamma = 1$ meV, was used for all electronic transitions.

perimentally obtained. It is important to notice that we used the constant lifetime γ_0 as an adjustable parameter and it was fixed to the value $\gamma_0 = 1$ meV.

The excitonic corrections to the Landau levels have been introduced in the results shown in Figs. 3–5 using the high-field limit as deduced in Ref. 12. As can be seen in Figs. 5(a)–5(b), there is an overestimation of the excitonic effects in our theoretical results, for low fields. This small difference was caused by the approximation, which is assumed in the method used to calculate the excitonic corrections to the resonances. In order to establish the importance of the magnetoexcitonic effects we show in Fig. 6 a comparison between Raman intensities calculated with and without excitonic corrections to Landau levels, for incident light at $\hbar\omega_L = 1620$ meV.

As a final comment, we also can observe some small shoulders in the experimental data to each side of a resonant peak. At present we have no explanation for these shoulders but are planning to more deeply analyze magneto-Raman spectroscopy and try to reach some conclusions about their possible origin.

VI. CONCLUSIONS

We have developed a microscopic theory for the magneto-Raman scattering for III-V and II-VI zinc-blende-type semiconductors in the framework of the Luttinger-Kohn Hamiltonian. The magneto-Raman transitions due to the electron-phonon deformation potential interaction are allowed in the crossed $\overline{z}(\sigma^{\pm},\sigma^{\mp})z$ geometries, even if the admixture through the Luttinger-Kohn Hamiltonian is taken into account.

The valence-band mixing in III-V and II-VI bulk semiconductors has strong influences on the Raman profile and on the shape of the resonant peaks. Under resonance, the Raman scattering efficiency increases as B_0^2 but the heights of the peaks are also influenced by the weights $a_{ij}(N,k_z)$, which measures the admixture of electronic states as well as

by the lifetime broadening for each intermediate state. The total lifetime broadening, γ_{NN}, for the electron-hole pair states, was calculated within the framework of the free electron-hole approach.

The calculated Raman efficiency intensity, according to the Luttinger-Kohn Hamiltonian, shows a number of new resonances related to the van Hove-like type of singularities in the density of the intermediate electron-hole states that could not be obtained with a simple parabolic model for the electronic structure. We stress that the calculation of the absolute value of the Raman scattering intensity is a complicated problem where the form of the electron-phonon interaction and the mixture of valence-band states play an important role in the determination of the shape of the spectra. The shift in the resonance energies as caused by the magnetoexciton effects was taken into account in the present work in the high field limit.

ACKNOWLEDGMENTS

V. L. acknowledges FAPESP for partial financial support of this work. G.E.M. acknowledges CNPq for partial financial support. The authors are indebted to T. Ruf who provided the experimental data used in this work.

*Also at Departamento de Física Teórica, Universidad de La Habana, 10400 C. Habana, Cuba.

[1] C. Trallero-Giner, T. Ruf, and M. Cardona, Phys. Rev. B **41**, 3028 (1990).

[2] C. R. Pigeon and R. N. Brown, Phys. Rev. **146**, 575 (1966).

[3] H. R. Trebin, U. Rössler, and R. Ranvaud, Phys. Rev. B **20**, 686 (1979).

[4] J. M. Luttinger, Phys. Rev. **102**, 1030 (1956).

[5] J. M. Luttinger and W. Kohn, Phys. Rev. **97**, 869 (1955).

[6] M. H. Weiller, in *Magneto Optical Properties of* $Hg_{1-x}Cd_xTe$ *Alloys*, edited by R. K. Willardson and A. C. Beer, Semiconductors and Semimetals, Vol. 16 (Academic Press, New York, 1966).

[7] A. Cantarero, C. Trallero-Giner, and M. Cardona, Phys. Rev. B **39**, 8388 (1989).

[8] G. L. Bir and G. E. Pikus, Fiz. Tverd. Tela **2**, 2287 (1960) [Sov. Phys. Solid State **2**, 2039 (1960)].

[9] C. Trallero-Giner, F. Iikawa, and M. Cardona, Phys. Rev. B **44**, 12 815 (1991).

[10] V. I. Belitsky, C. Trallero-Giner, and M. Cardona, Phys. Rev. B **41**, 3039 (1990).

[11] T. Ruf, Ph.D. thesis, Max-Planck-Institut für Festkörperforschung Stuttgart, 1990.

[12] T. Ruf, R. T. Phillips, A. Cantarero, G. Ambrazeviçius, M. Cardona, J. Schmitz, and U. Rössler, Phys. Rev. B **39**, 13 378 (1989).

[13] *Semiconductors. Physics of Group IV Elements and III-V Compounds*, edited by O. Madelung, M. Schultz, and H. Weiss, Landolt-Börnstein, New Series, Group III, Vol. 17, Pt. a (Springer-Verlag, Berlin, 1982).